Complement C5 inhibition protects against hemolytic anemia and acute kidney injury in anthrax peptidoglycan-induced sepsis in baboons

Ravi Shankar Keshari[a,1], Narcis Ioan Popescu[b,1], Robert Silasi[a], Girija Regmi[a], Cristina Lupu[a], Joe H. Simmons[c], Alonso Ricardo[d], K. Mark Coggeshall[b,2], and Florea Lupu[a,e,f,g,2,3]

[a]Cardiovascular Biology Research Program, Oklahoma Medical Research Foundation, Oklahoma City, OK 73104; [b]Arthritis and Clinical Immunology Research Program, Oklahoma Medical Research Foundation, Oklahoma City, OK 73104; [c]Michale E. Keeling Center for Comparative Medicine and Research, University of Texas MD Anderson Cancer Center, Bastrop, TX 78602; [d]Ra Pharmaceuticals Inc., Cambridge, MA 02140; [e]Department of Cell Biology, University of Oklahoma Health Sciences Center, Oklahoma City, OK 73104; [f]Department of Pathology, University of Oklahoma Health Sciences Center, Oklahoma City, OK 73104; and [g]Department of Internal Medicine, University of Oklahoma Health Sciences Center, Oklahoma City, OK 73104

Edited by Arturo Casadevall, Johns Hopkins University, Baltimore, MD, and accepted by Editorial Board Member John Collier July 14, 2021 (received for review March 8, 2021)

Late-stage anthrax infections are characterized by dysregulated immune responses and hematogenous spread of *Bacillus anthracis*, leading to extreme bacteremia, sepsis, multiple organ failure, and, ultimately, death. Despite the bacterium being nonhemolytic, some fulminant anthrax patients develop a secondary atypical hemolytic uremic syndrome (aHUS) through unknown mechanisms. We recapitulated the pathology in baboons challenged with cell wall peptidoglycan (PGN), a polymeric, pathogen-associated molecular pattern responsible for the hemostatic dysregulation in anthrax sepsis. Similar to aHUS anthrax patients, PGN induces an initial hematocrit elevation followed by progressive hemolytic anemia and associated renal failure. Etiologically, PGN induces erythrolysis through direct excessive activation of all three complement pathways. Blunting terminal complement activation with a C5 neutralizing peptide prevented the progressive deposition of membrane attack complexes on red blood cells (RBC) and subsequent intravascular hemolysis, heme cytotoxicity, and acute kidney injury. Importantly, C5 neutralization did not prevent immune recognition of PGN and shifted the systemic inflammatory responses, consistent with improved survival in sepsis. Whereas PGN-induced hemostatic dysregulation was unchanged, C5 inhibition augmented fibrinolysis and improved the thromboischemic resolution. Overall, our study identifies PGN-driven complement activation as the pathologic mechanism underlying hemolytic anemia in anthrax and likely other gram-positive infections in which PGN is abundantly represented. Neutralization of terminal complement reactions reduces the hemolytic uremic pathology induced by PGN and could alleviate heme cytotoxicity and its associated kidney failure in gram-positive infections.

peptidoglycan | anthrax | complement | acute kidney injury | hemolysis

The spore-forming, gram-positive *Bacillus anthracis* (1) causes a disease that mainly affects grazing herbivores. Whereas the incidence of the natural anthrax in humans is low (2), the expansion of the ecological niche (3), weaponization of anthrax spores (4), and the horizontal transfer of virulence plasmids to related bacteria (5, 6) increases the risk of pathogen exposure. If diagnosed early, anthrax infections are efficiently treated with antibiotics. In contrast, the fulminant disease stage is more refractory to therapeutics resulting in high mortality (1). In addition, isolates of *Bacillus cereus biovar anthracis* (*Bcbva*) promote anthrax pathology while displaying *Bacillus cereus* antibiotic sensitivities (7, 8), raising the chance of disastrous emergence of antibiotic resistant anthrax variants.

Anthrax progression is driven by virulence factors such as the poly-γ-D-glutamate capsule (9) and anthrax toxins (10), which support evading host immunity to cause systemic bacterial dissemination. The fulminant phase of the disease is characterized by extreme bacteremia and sepsis pathophysiology including fever, anomalous leukocyte counts, systemic inflammation, hemostatic dysregulation, multiple organ failure, and death (11–13). Anthrax sepsis is recapitulated in nonhuman primates (NHP) challenged intravascularly with either *B. anthracis* (14) or the cell wall peptidoglycan (PGN) devoid of any other bacterial PAMPs (pathogen-associated molecular patterns) (15). Unlike anthrax toxins, PGN induces anthrax-associated coagulopathy through activation of both the extrinsic and intrinsic coagulation cascades and consumption of natural inhibitors (15), promoting disseminated intravascular coagulation (DIC) pathology in fulminant anthrax (16).

PGN is the major constituent of the cell wall of gram-positive pathogens (17). It is a polymer of crosslinked linear glycans having repeat disaccharide units of N-acetyl glucosamine and N-acetyl muramic acid. PGN diversity relies on the heterogeneity of the crosslinking peptide bridges and secondary carbohydrate modifications, which modulate their recognition by immune receptors (18–20).

Significance

Late-stage anthrax leads to sepsis, characterized by uncontrolled host responses that contribute to organ damage and death. Using a nonhuman primate model, we demonstrate that bacterial wall peptidoglycan is the major trigger of complement activation. Terminal complement activation products promote secondary hemolytic uremic syndrome (HUS), characterized by hemolytic anemia, toxic accumulation of iron in the kidneys, and subsequent acute renal injury. Inhibition of C5 cleavage and subsequent formation of the lytic terminal complex C5b-9 prevented intravascular hemolysis and heme cytotoxicity and protected against peptidoglycan-induced acute kidney failure. Overall, treatment with C5 inhibitor significantly improved the survival of baboons with sepsis, suggesting a potentially important strategy to treat HUS secondary to gram-positive bacterial infections.

Author contributions: R.S.K., N.I.P., C.L., K.M.C., and F.L. designed research; R.S.K., N.I.P., R.S., G.R., C.L., J.H.S., and F.L. performed research; A.R. contributed new reagents/analytic tools; R.S.K., N.I.P., R.S., G.R., C.L., J.H.S., K.M.C., and F.L. analyzed data; and R.S.K., N.I.P., K.M.C., and F.L. wrote the paper.

This article is a PNAS Direct Submission. A.C. is a guest editor invited by the Editorial Board.

Competing interest statement: A.R. was employed by Ra Pharmaceuticals at the time that the work was conducted. Data presented in this report make the subject of a preliminary patent application.

[1]R.S.K. and N.I.P. contributed equally to this work.

[2]K.M.C. and F.L. contributed equally to this work.

[3]To whom correspondence may be addressed. Email: florea-lupu@omrf.org.

This article contains supporting information online at https://www.pnas.org/lookup/suppl/doi:10.1073/pnas.2104347118/-/DCSupplemental.

Published September 10, 2021.

We have extensively studied innate recognition of anthrax PGN and the subsequent cellular immune responses. Anthrax PGN is not recognized by surface Toll-like receptors (21) but rather interacts with professional phagocytes through immunoglobulin and/or C3 complement receptors (22–24). Optimal immune responses require PGN internalization, lysosomal processing (25), and activation of intracellular NOD sensors (18, 19). PGN can also signal through activating surface Fc receptors (22, 26). Anthrax PGN induces proinflammatory and procoagulant responses in human monocytes (25, 27, 28), degranulation, and inflammatory responses in neutrophils (24, 29) and platelet aggregation (23). Furthermore, PGN activates blood coagulation in primates (15) and the human complement cascade ex vivo (30). In NHPs, PGN challenge recapitulates the pathophysiology of late-stage anthrax sepsis including systemic inflammation, progressive coagulopathy, imbalanced vascular permeability, multiple organ dysfunction, and death (15). Since anthrax PGN is free of other PAMPs, these studies therefore model sepsis caused by other clinically relevant gram-positive pathogens.

Our study highlights the role of the terminal complement mediators in hemolysis-associated organ damage during late-stage anthrax. While the bacterium is considered nonhemolytic in bacteriological tests (7), hemolytic anemia has been reported in both inhalational (13) and cutaneous (31) anthrax patients. Because *B. anthracis* does not secrete hemolysins, an earlier study proposed that anthrax toxins initiate erythrolysis through an unknown neutrophil mediated mechanism (32). The relevance of such a mechanism for human pathology is questionable, however, since hemolytic anemia was reported in patients treated with antibiotics (13, 31), which gradually decrease circulating toxin levels (33). Here we show that NHPs challenged with anthrax PGN elicit hematocrit dynamics similar to humans, with an initial elevation followed by progressive erythrolysis. The resulting heme imbalance leads to toxic accumulation of iron in kidneys and subsequent acute renal injury.

We previously reported that RA101295, a specific complement C5 inhibitor, protects NHPs from a lethal *Escherichia coli* challenge (30). RA101295 is a small (~2 kDa), 15–amino acid macrocyclic peptide that binds to C5 with high affinity and specificity and inhibits cleavage of C5 by the classical (CP), lectin (LP), or alternative pathway (AP) C5 convertases, hence blocking the generation of the bioactive split-products C5a and C5b as well as C5b binding to complement component C6. This dual inhibitory mechanism prevents both the generation of the potent C5a anaphylatoxin and the assembly of the terminal C5b-9 complement complex. Treatment with RA101295 prevented the release of lipopolysaccharide (LPS) after extracellular bacteriolysis and subsequently reduced systemic inflammation, coagulopathy, and the associated organ damage (30). Since C3 activation is important for opsono-phagocytosis of vegetative *B. anthracis* (24) and its spores (24, 34), we hypothesized that inhibition of the complement cascade downstream of C3 activation, important for immune recognition of PGN (24), could prevent complement driven pathologies in gram-positive PGN sepsis without impairment of innate immune responses. In this study, we show that RA101295 prevents intravascular and extravascular hemolysis, reduces accumulation of iron and pathologic deposition of C5b-9 terminal complement complexes, and protects against multiple organ failure and death in NHPs challenged with anthrax PGN.

Results

Effect of RA101295 on Clinical Signs of Sepsis in PGN-Challenged Baboons. Fever, tachycardia, hypotension, and impaired blood oxygenation are more commonly observed in inhalational anthrax than common respiratory infections (35). A similar symptomatology was observed in PGN-challenged baboons. RA101295 treatment did not change the core body temperature dynamics but slightly improved the cardiopulmonary responses of the animals while under anesthesia and prevented PGN-induced hypotensive shock (*SI Appendix*, Fig. S1).

Effect of RA101295 on PGN-Induced Complement Activation. PGN induced the activation of all three complement pathways in vivo, CP, LP, and AP, as assessed by the pathway-specific residual complement activities (Fig. 1*A*). One hour after the PGN infusion, we observed a complete consumption of AP (3.26% residual AP activity, $P = 0.003$, RM one-way ANOVA) and significant reduction in CP and LP residual activities (25.11% residual CP activity, $P = 0.0407$, and 23.05% residual LP activity, $P = 0.0313$, respectively). We conclude that PGN rapidly activates the complement system leading to acute consumption of complement C3. Roughly 50% complement activity was recovered for all three pathways by 8 h post challenge, which likely reflects de novo C3 biosynthesis. AP recovery accelerates and reaches a maximum of 40% above T0 baseline at 48 h. CP showed a similar but delayed recovery, returning to baseline potential by 48 h and 40% above baseline by 72 h postchallenge. LP was the slowest to recover, lingered at 50% activity for the first 48 h, and only returned to baseline levels at 72 h postchallenge. The results suggest either a slower biosynthesis of LP specific components or prolonged activation of LP.

The PGN challenge led to rapid elevation of complement activation products, such as C3b, C5a, and sC5b-9, which peaked as soon as 1 h after the PGN infusion (Fig. 1 *B–D*). RA101295 strongly decreased plasma C5a levels and completely abrogated circulating sC5b-9 at all time-points (Fig. 1 *C–D*). As expected, RA101295 did not inhibit C3 proteolysis, and we detected higher levels of C3b in RA101295-treated baboons. Excessive complement activation led to pathologic deposition of the terminal C5b-9 complement complex (membrane attack complex, MAC) in host tissues. We observed deposition on erythrocytes as early as 2 h post PGN infusion and MAC accumulation in multiple peripheric tissues collected at endpoint (Fig. 1*E*). RA101295 treatment significantly reduced pathologic MAC deposition on host cells in all animals enrolled in the study.

Effect of RA101295 on PGN-Induced Hemolysis. Anthrax patients usually present with elevated hematocrit (>45%) (13, 35), which precipitously decreases in hemolytic patients (13, 31) who then require compensatory blood transfusions. PGN-challenged baboons displayed a rapid increase in erythrocyte counts, hematocrit, and hemoglobin levels (Fig. 2 *A–C*), followed by a steady decrease of all parameters within 8 to 72 h post challenge. While the hematocrit elevation was not significantly different in the RA101295-treated, PGN-challenged, baboons it was generally lower in the treated group with only one animal showing ≥22% elevation. In contrast, three of four PGN-challenged baboons showed hematocrit values ≥30% above baseline in the absence of treatment. During the hemolytic stage of the challenge, the RA101295 inhibitor protected against hemolysis and stabilized erythrocyte numbers at ~80% of baseline (Fig. 2*B*).

Concurrently, schistocytes, irregular shaped red blood cells (RBC), and erythrocyte ghosts devoid of hemoglobin were detected microscopically on peripheral blood smears collected 24 to 72 h post PGN infusion. At later time-points, lysed and/or aggregated RBCs were also observed (Fig. 2*D*). RA101295 reduced schistocytosis and RBC aggregation (Fig. 2*D*) and similarly reverted the hemoglobinemia regularly observed in plasma samples collected after 8 h post PGN infusion. Plasma bilirubin dynamics confirmed the protective effects of RA101295 against the intravascular heme imbalance induced by the PGN challenge (Fig. 2*E*). Damaged RBCs are cleared from circulation by phagocytic macrophages in spleen or liver which recycle hemin groups. PGN enhanced extravascular hemolysis, as evidenced by increased deposition of iron in perifollicular regions of the spleen (Fig. 2*F*), while RA101295 lessened extravascular hemolysis and lowered iron accumulation in these organs.

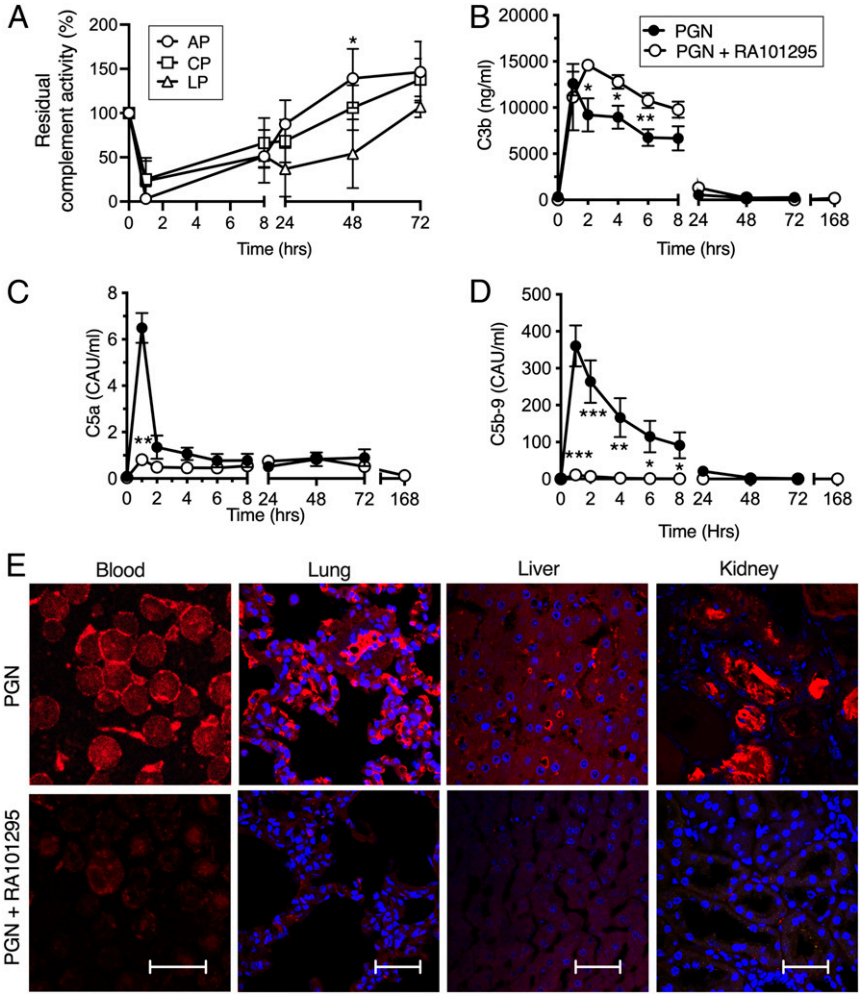

Fig. 1. Effect of RA101295 treatment on complement activation and C5b-9 deposition in tissues following infusion of a lethal dose of PGN. (*A*) Time course changes of complement components that support complement activation via AP, CP, and LP in serial serum samples shows rapid consumption of complement proteins after 1 h post PGN infusion in baboons. A faster recovery of AP was observed (*$P < 0.05$, LP versus AP, 48 h post PGN challenge). (*B–D*) Quantitation of complement activation products in serial plasma samples collected from PGN-challenged baboons: (*B*) Soluble C3b, (*C*) soluble C5a, (*D*) and soluble C5b-9. Data are presented as mean ± SEM. The same time-points from PGN ($n = 4$) and PGN+RA101295 ($n = 3$) were compared using two-tailed Student's *t* test. *$P < 0.05$, **$P < 0.01$, and ***$P < 0.001$. (*E*) Immunostaining for C5b-9 (red) and nuclear counterstaining (blue, TO-PRO-3) in lung, liver, and kidney sections of PGN-challenged baboons euthanized at 72 h (untreated) or 7 d (RA101295 treated). Left depicts C5b-9 immunostaining performed on blood smears collected 2 h post PGN challenge in both untreated and RA101295 treated baboons. (Magnification bars: 20 μm [blood]; 50 μm [lung, liver, and kidney].)

Effect of RA101295 on Organ Dysfunction. PGN challenge induced anatomopathological changes and functional impairment of multiple organs (*SI Appendix*, Figs. S2 and S3). PGN-induced thrombosis and subsequent organ damage has been detailed previously (15). Kidneys were the most severely affected organs, and acute renal failure in conjunction with progressive hyperkalemia was the most likely cause of death for these animals. Kidney dysfunction was initiated early, with BUN (blood urea nitrogen) and creatinine levels above physiologic range as early as 8 h after PGN infusion. Renal impairment worsened throughout the course of the experiment, reaching 11- to 14-fold increases over baseline for BUN (154 to 280 mg/dL) and 26- to 29-fold increases for creatinine (9.3 to 13.7 mg/dL) by 72 h in 3/4 PGN-challenged baboons (Fig. 3*A*). Kidney dysfunction led to a concomitant elevation in blood potassium to life-threatening levels above 7 mM. RA101295-treated animals elicit a similar elevation in BUN and creatinine during the first 8 h post challenge. In contrast to nontreated animals, however, kidney dysfunction stabilizes by 24 h and improves afterward (Fig. 3*A*). Correspondingly, blood potassium never exceeded 5.4 mM in any of the RA101295-treated baboons.

Endpoint histopathological analysis of PGN -hallenged baboons revealed thrombo-ischemia and hemoglobinemia-induced acute tubular necrosis. Hematoxylin and eosin–stained kidney sections showed damage to the epithelial cells of proximal tubules and disorganization of their nuclei (karyolysis), glomerular necrosis, and accumulation of leukocytes in the peritubular capillaries of PGN-challenged animals (Fig. 3*B*). Thrombo-ischemic damage of glomerular and peritubular capillaries has been reported previously (15) and is exemplified in *SI Appendix*, Fig. S3 as well. Intravascular hemolysis releases heme in circulation, which sensitizes parenchyma to regulated necrosis in the presence of proinflammatory stimuli (36, 37). Acute kidney injury is an early manifestation of heme cytotoxicity in vivo (38), it is dominated by kidney tubular necrosis (39) and amplifies multiple organ dysfunction in polymicrobial sepsis (40). Following intravascular hemolysis, we observed widespread accumulation of hemosiderin in the renal tubules of PGN-challenged baboons (Fig. 3*C*), and the renal damage was amplified by MAC deposition. Colocalization of C5b-9 with immunoglobulins (Fig. 3*D*), factor B (Fig. 3*E*), and/or MBL (Fig. 3*F*) indicates CP-, AP-, and LP-dependent renal MAC deposition. RA101295

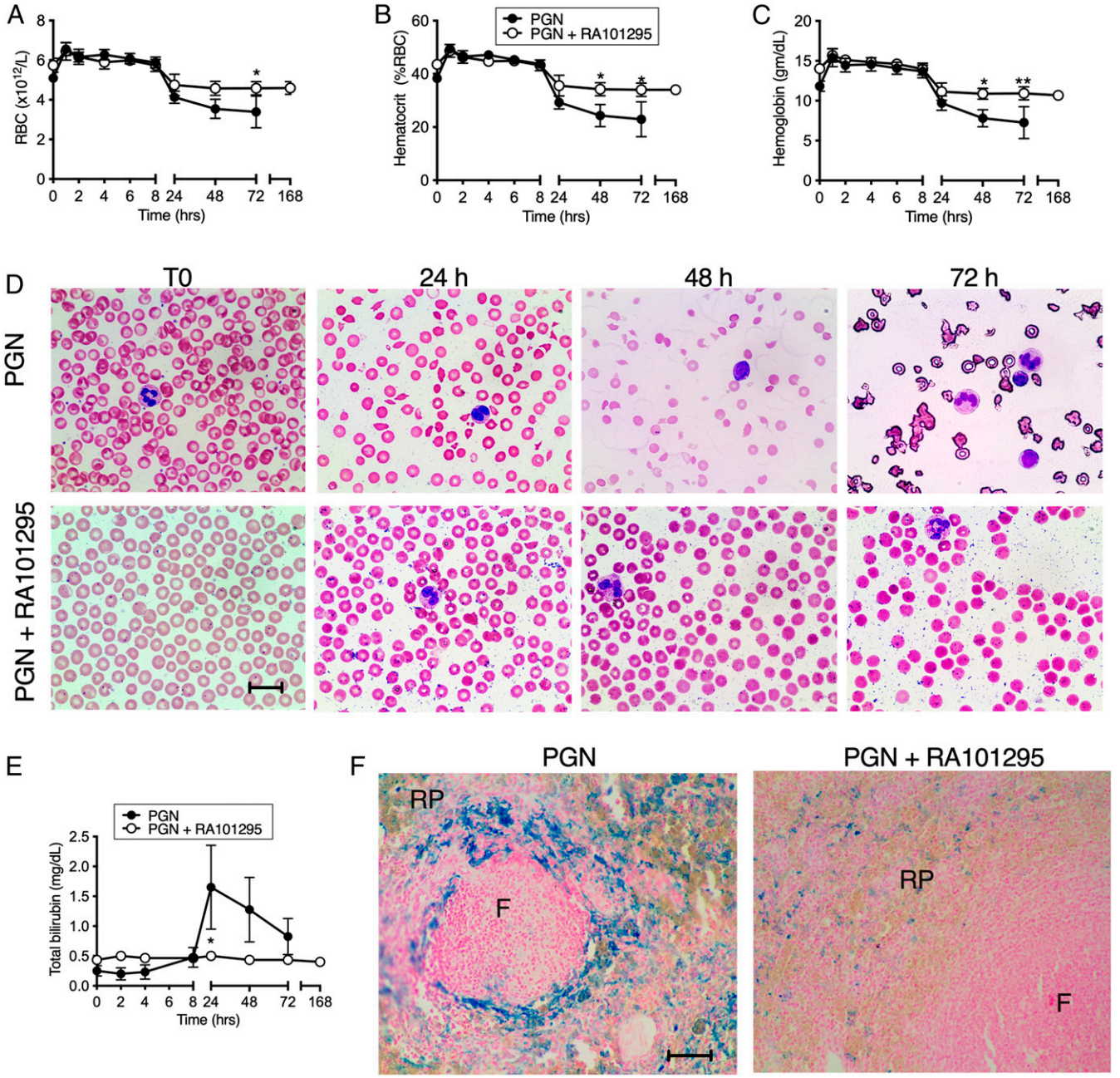

Fig. 2. Effect of RA101295 on intravascular and extravascular hemolysis induced by PGN. (*A–E*) Time course dynamics of RBC counts (*A*), hematocrit (*B*), hemoglobin (*C*), erythrocyte morphology (*D*), and total bilirubin (*E*). Gradual increase in schistocytes and aggregated ghost RBCs in PGN-challenged, untreated baboons was noted prominently at 72 h (*D*, *Right*), while treated baboons were protected against hemolysis. (*F*) Prussian blue staining of hemoglobin-derived iron deposits in the spleen of PGN challenged baboons without/with RA101295 treatment. Deposition of blue-stained colloidal iron was observed in the red pulp (RP), particularly in the areas surrounding the follicles (F). RA101295-treated animals did not show iron staining, suggesting decreased extravascular RBC hemolysis in the spleen. (*A–C*, *E*) Data are presented as mean ± SEM, and the same time-points are compared between PGN ($n = 4$) and PGN+RA101295 ($n = 3$) using two-tailed Student's *t* test. $^*P < 0.05$, $^{**}P < 0.01$. (Magnification bars: 20 μm [*D*]; 100 μm [*F*].)

treatment reduced PGN-induced MAC deposition in the kidney, lowered heme cytotoxicity and the accumulation of renal hemosiderin, and decreased but did not eliminate tubular necrosis (Fig. 3 *B–F*, lower panels). Occlusive thrombi in glomerular capillaries, interlobular arteries, and peritubular capillaries were only occasionally observed in the RA101295 treated group.

Effect of RA101295 on Leukocyte Activation during PGN Challenge. Anthrax patients developing hemolytic anemia show concurrent leukopenia, thrombocytopenia, and progressive coagulopathy (13, 31). Similar to human pathology, PGN induced platelet decline in baboons during the first 8 h after infusion, with gradual recovery afterward in both experimental groups (Fig. 4*A*). Similarly, leukocytes (white blood cells, WBCs) declined steeply to 40 to 50% of baseline within 2 h after PGN infusion but recovered to or above baseline by 24 h. No significant changes in WBC dynamics were observed between RA101295-treated and untreated groups (Fig. 4*B*).

PGN infusion promoted rapid engagement and degranulation of neutrophils as indicated by the increased plasma myeloperoxidase (MPO) activity. MPO peaked early, 1 to 2 h after the challenge

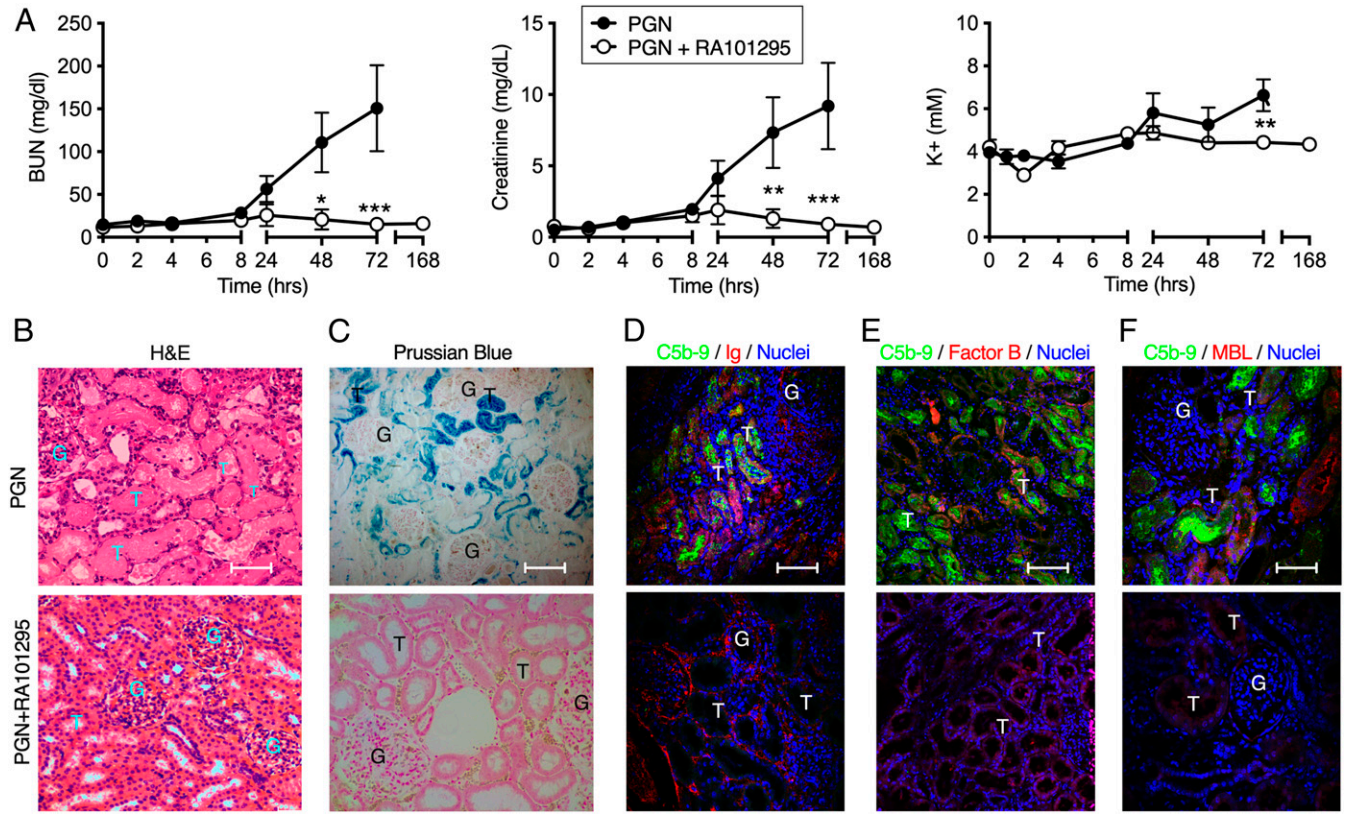

Fig. 3. Effect of RA101295 treatment on markers of renal injury, including complement and iron deposition, following infusion of a lethal dose of PGN. (*A*) Time course dynamics of serum BUN and creatinine in untreated or RA101295-treated baboons challenged with anthrax PGN. Data are presented as mean ± SEM. The same time-points are compared between PGN ($n = 4$) and PGN+RA101295 ($n = 3$) using two-tailed Student's *t* test. $^{*}P < 0.05$, $^{**}P < 0.01$, and $^{***}P < 0.001$. (*B*) Hematoxylin and eosin (H&E) staining of kidney sections reveals extensive tubular necrosis in nontreated animals, while RA101295 treatment protected the morphological integrity of the organ. (*C*) Perl's Prussian blue staining of ferric iron (Fe^{3+}) hemosiderin deposits in tubules of kidney. (*D*, *E*, and *F*) Double immunolabeling of immunoglobulins (Ig; *D*, red), factor B (*E*, red), or mannose-binding lectin (MBL; *F*, red) and C5b-9 terminal complement complex (*D*, *E*, and *F*, green). In all pictures, TO-PRO-3 nuclear counterstaining is shown in blue. *G*, glomeruli; T, tubule. (Magnification bars: 100 μm.)

(Fig. 4*C*), and was sustained after RA101295 treatment, consistent with the enhanced activation of C3 in these animals (Fig. 1*B*), and our previous observations that C3b opsonization supports neutrophil recognition of both anthrax bacterium and PGN (24). RA101295-treated baboons have significantly lower levels of monocyte/macrophage activation marker neopterin at 24 to 72 h post PGN challenge (Fig. 4*D*). Neopterin is eliminated through the kidney (41), and time course dynamics are similar to the kidney dysfunction marker creatinine (Fig. 3*A*). Time course dynamics of granzyme B, a NK cells/cytotoxic T cells activation marker, is similar in both groups (Fig. 4*E*). Nucleosomes are complexes of DNA and histones released by either activated neutrophils, in the form of neutrophil extracellular traps (NETs), or damaged apoptotic or necrotic cells. Circulating nucleosomes sharply increased within the first 8 h after PGN infusion in both RA101295-treated and untreated animals. During challenge resolution, 24 to 72 h post infusion, RA101295 treatment significantly reduced circulating nucleosome levels, highlighting the cytoprotective effects of C5 inhibition (Fig. 4*F*). Overall, the results indicate that C5 inhibition does not alter PGN interaction with circulating innate immune cells, supports similar neutrophil responses like degranulation, and is cytoprotective during the resolution phase of the PGN challenge.

Effect of RA101295 on PGN-Induced Systemic Inflammation. Our previous studies showed that PGN can induce systemic inflammation similar to the parental bacteria (15). RA101295 treatment did not alter PGN-induced production of inflammatory mediators responsible for myeloid cell mobilization, such as GM-CSF (granulocyte macrophage colony-stimulating factor) and MCP-1 (monocyte chemoattractant protein 1) (Fig. 5 *A*–*B*). While RA101295 treatment did not affect PGN-induced TNF or IL-8 dynamics (Fig. 5 *C* and *E*), it significantly reduced IL-6 at later stages (Fig. 5*D*), reflecting potentiation of IL-6 biosynthesis through either C5 anaphylatoxin (42) or sublytic C5b-9 (43) signaling. Surprisingly, C5 inhibition enhanced the biosynthesis of the pleiotropic cytokine IFN-γ (interferon-gamma) (Fig. 5*F*). Similar to IL-6, the initial up-regulation of the regulatory cytokines IL-10 and IL1-RA (IL-1 receptor antagonist) was unchanged, while both were reduced by C5 inhibition at later stages (Fig. 5 *G*–*H*).

Effect of RA101295 Treatment on Plasma Levels of PGN Recognition Proteins. Mammals express four PGN recognition proteins (PGLYRPs) that interact with PGN, two of which (PGLYRP1 and 2) are released in the blood. PGLYRP1 has bactericidal activity and supports PGN signaling, while PGLYRP2 has amidolytic activity and mediates PGN degradation (44). We measured changes in plasma levels of PGLYRP1 and PGLYRP2 in baboons challenged with PGN, with/without RA101295 treatment. PGLYRP1 is constitutively produced and stored as ~22 kDa monomers in the tertiary granules of neutrophils, and dimerization increases its efficiency and specificity (45). We detected PGLYRP1 only as a dimer in NHP plasma, visible after 2 to 8 h post PGN infusion and likely reflecting neutrophil activation and degranulation. RA101295-treated animals showed lower levels of PGLYRP1 as compared to nontreated controls (*SI Appendix*, Fig. S4*A*).

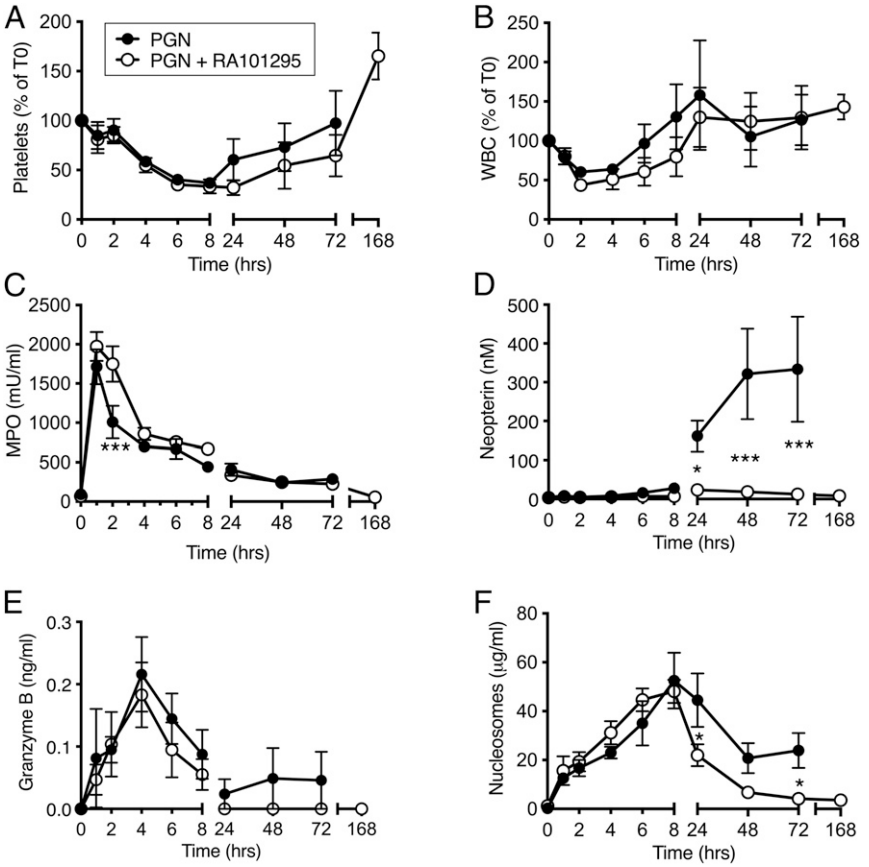

Fig. 4. Effect of RA101295 treatment on platelets and leukocytes counts and markers of leukocyte activation following a lethal PGN challenge. Time course dynamics of platelets (*A*), WBCs (*B*), MPO (*C*), neopterin (*D*), granzyme B (*E*), and nucleosomes (*F*) in serial blood samples collected from PGN challenged baboons with or without RA101295 treatment. Data are presented as mean ± SEM, and the same time-points are compared between PGN ($n = 4$) and PGN+RA101295 ($n = 3$) using two-tailed Student's *t* test. $^{*}P < 0.05$, $^{***}P < 0.001$.

PGN challenge with or without RA101295 treatment did not significantly change the expression of PGLYRP2, a liver deaminase enzyme that is constitutively secreted in plasma, in which it can cleave and degrade PGN, thus contributing to its clearance (*SI Appendix*, Fig. S4*B*).

Effect of C5 Inhibition on PGN-Induced Coagulopathy. Acquired hemolytic anemia with schistocytosis, as observed here, occurs more frequently in patients with progressive coagulopathy, DIC, and thrombotic microangiopathies (46). As reported (15), PGN-challenged baboons exhibited an acute consumptive coagulopathy characterized by prolonged clotting times, aPTT (activated partial thromboplastin time; Fig. 6*A*) and PT (prothrombin time, Fig. 6*B*), elevation of thrombin-antithrombin complexes (Fig. 6*C*), and consumption of fibrinogen (Fig. 6*D*). RA101295 treatment did not significantly alter any of these parameters indicating that C5 inhibition has no substantial effect on the hemostatic dysregulation induced by PGN (Fig. 6). Accordingly, the RA101295 treatment reduced but did not eliminate glomerular and peritubular microthrombi in PGN-challenged baboons (*SI Appendix*, Fig. S3), resulting in mild renal impairment up to 48 h post challenge (Fig. 3*A*). PGN activates both the intrinsic (contact) and extrinsic (tissue factor–dependent) coagulation cascades (15), and we detected pathway-specific protease–serpin complexes in this study as well (Fig. 6 *E*–*G*) and kininogen consumption (Fig. 6*H*). While the overall dynamics are similar, the peaks of protease–serpin complexes were delayed by roughly 1 h in RA101295-treated versus untreated PGN-challenged baboons.

RA101295 had no effect on the fibrinolytic activator tPA (tissue plasminogen activator; Fig. 6*I*), nor the corresponding regulator PAI-1 (plasminogen activator inhibitor 1; Fig. 6*J*), although plasmin–antiplasmin (PAP) complexes were slightly higher in the treated group (Fig. 6*K*). Surprisingly, the fibrin-specific degradation product D-dimer was significantly elevated in the RA101295-treated, PGN-challenged animals, especially 24 h post infusion (Fig. 6*L*). The enhanced fibrinolysis observed in RA101295-treated animals is expected to ease the thrombo-ischemic injury induced by PGN.

Endothelial injury usually precedes thrombotic microangiopathies and the associated intravascular hemolysis. Quantitation of soluble thrombomodulin (sTM; Fig. 6*M*) confirmed the cytoprotective effects of C5 inhibition on vascular endothelium. Temporal dynamics of sTM indicates that PGN-induced endothelial injury is due in part to the excessive activation of terminal complement mediators within vasculature and not the heme imbalance observed at later time-points. TM release was reduced but not abolished by RA101295, reflecting concomitant endothelial activation by thrombin or systemic inflammation largely unaffected by C5 inhibition.

Effect of RA101295 on Survival. Without treatment, the PGN challenge led to irreversible organ failure, triggering euthanasia between 72 and 111 h post infusion (mean survival: 96 h). Inhibition of terminal complement mediators by RA101295 protected against pathologic complement deposition on blood cells and peripheric organs, reduced intravascular hemolysis, and associated heme-mediated renal injury. RA101295-treated, PGN-challenged baboons

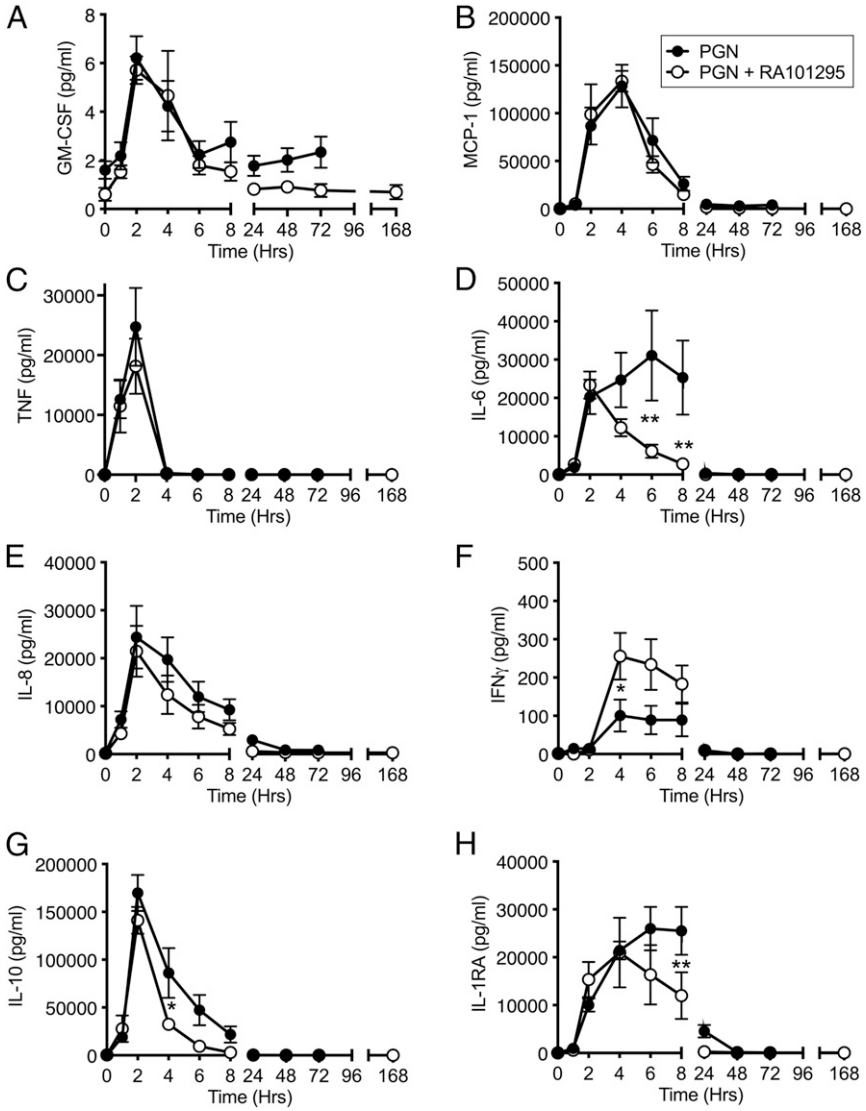

Fig. 5. Effect of RA101295 treatment on inflammatory cytokines production following a lethal dose of PGN infusion. Time course of circulating cytokines: GM-CSF (granulocyte-macrophage colony-stimulating factor) (*A*), MCP-1 (monocyte chemoattractant protein 1) (*B*), TNF (*C*), IL-6 (*D*), IL-8 (*E*), IFN-γ (*F*), IL-10 (*G*), and IL-RA (IL-1 receptor antagonist) (*H*). Data are presented as mean ± SEM. The same time-points are compared between PGN ($n = 4$) and PGN+RA101295 ($n = 3$) using two-tailed Student's *t* test. $^{*}P < 0.05$, and $^{**}P < 0.01$.

reached the 7-d endpoint of the study and were considered survivors (Fig. 7).

Discussion

PGN is an abundant component of gram-positive bacterial wall from which is shed during the vegetative growth (47) or after bacteriolysis induced by antibiotics (48) or lysozyme (49). We recently showed that PGN supports the anthrax-associated coagulopathy, which is characterized by progressive thrombocytopenia, DIC, occlusive microthrombosis, and multiple organ dysfunction (15). Here, we found that PGN-challenged baboons also elicits a secondary atypical hemolytic uremic syndrome (aHUS) pathology characterized by an initial hematocrit elevation, characteristic of clinical anthrax presentation (35), followed by progressive hemolytic anemia, thrombocytopenia, and acute kidney injury, and we investigated the underlying pathological mechanisms. We show here that excessive activation of terminal complement caused intravascular hemolysis during the PGN challenge. Inhibition of C5 cleavage by RA101295 abrogated terminal complement reactions without affecting upstream activation. C5 inhibition reduced intravascular hemolysis, heme cytotoxicity, and associated renal injury, with no adverse effects on cellular innate immune responses, systemic inflammation, or coagulopathy. Consequently, C5 inhibition protected against acute kidney failure and promoted survival in baboons challenged with a lethal dose of anthrax PGN.

Hemolytic anemia in critically ill septic patients usually associates with adverse outcomes (50, 51). Acquired HUS predominantly accompanies infections with enterohemorrhagic *E. coli*, whereby the pathology is driven by bacterial Shiga toxins (52). The mechanisms supporting HUS in gram-positive infections (53) are less understood. The true incidence of HUS in human anthrax is difficult to assess due to the low occurrence of bacteremic natural anthrax cases; however, one out of the first 10 cases in the Amerithrax attack developed HUS (13), and HUS developments were reported in community acquired cutaneous (31) and inhalational (54) anthrax. Here, we show that baboons challenged intravascularly with anthrax PGN developed a progressive hemolytic anemia similar to human patients. The initial hematocrit elevation is likely due to altered vascular permeability (15) and

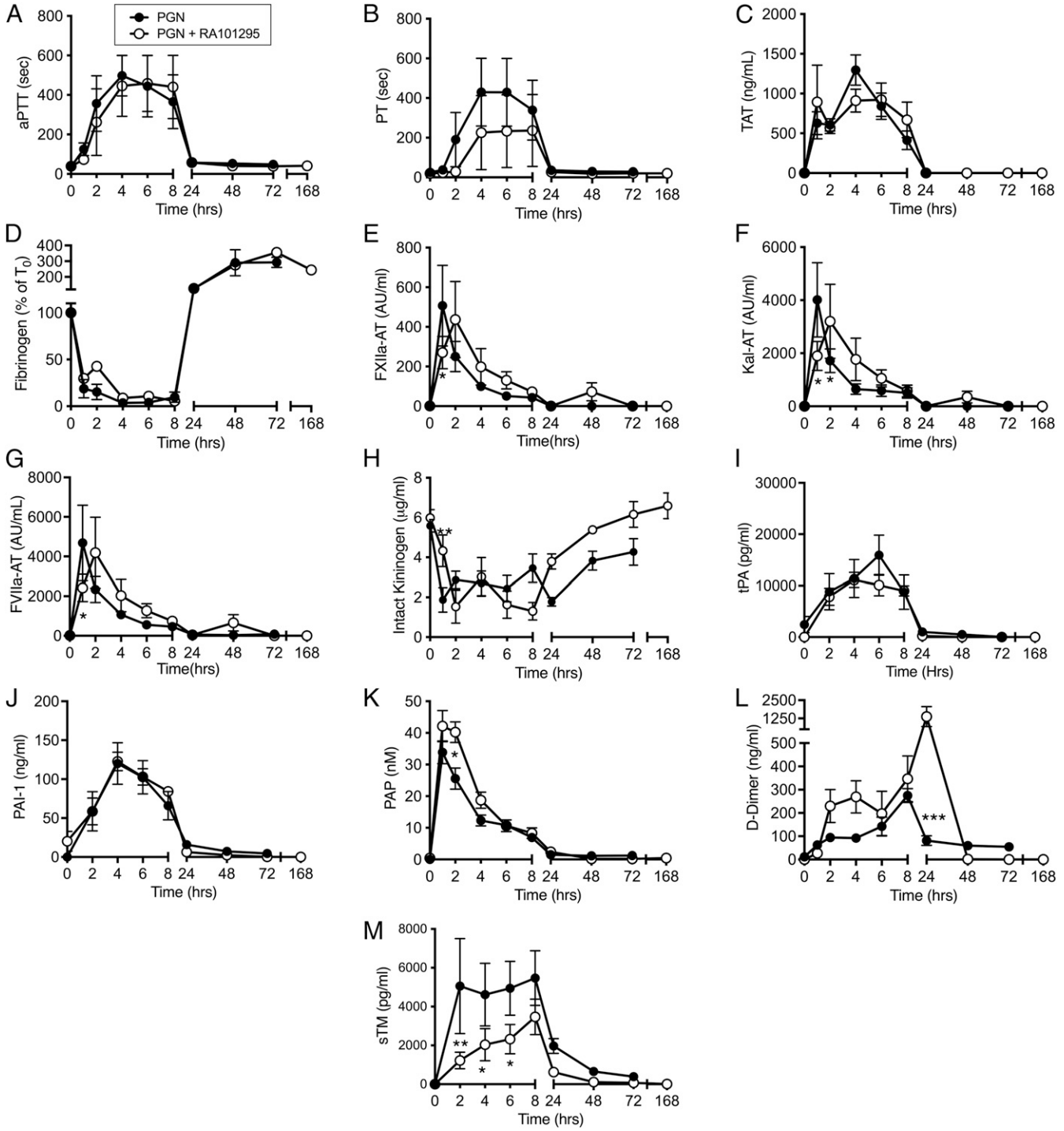

Fig. 6. Effect of RA101295 on markers of coagulation and fibrinolysis following PGN challenge. Time course dynamics of activated partial thromboplastin time (aPTT; *A*), prothrombin time (PT; *B*), thrombin-antithrombin complexes (TAT; *C*), fibrinogen (*D*), FXIIa-AT complexes (*E*), Kallikrein-AT complexes (*F*), FVIIa-AT complexes (*G*), intact kininogen (*H*), tissue type plasminogen activator (tPA; *I*), plasminogen activator inhibitor-1 (PAI-1; *J*), plasmin-α2–antiplasmin complexes (PAP; *K*), D-dimers (*L*), and soluble thrombomodulin (sTM; *M*) in PGN challenged baboons with or without RA101295 treatment. Data are depicted as mean ± SEM, and the same time-points are compared between PGN ($n = 4$) and PGN+RA101295 ($n = 3$) using two-tailed Student's *t* test. $^{*}P < 0.05$, $^{**}P < 0.01$, and $^{***}P < 0.001$.

hemoconcentration, while excessive complement activation drives hemolysis at later stages.

Understanding the pathologic mechanisms promoting infection-associated hemolytic anemia can inform targeted therapeutic strategies. Possible etiologies for bacteria-driven anemia include secretion of pathogen-derived hemolysins, DIC and thrombotic microangiopathies, dysregulated complement activation, glucose restriction, alterations in RBC deformability, and others (55, 56). The mechanisms supporting anthrax-associated HUS pathology are unknown. Unlike the closely related *B. cereus* (57), anthrax does not secrete hemolysins and consequently is classified as gamma-hemolytic (nonhemolytic) in standard bacteriological

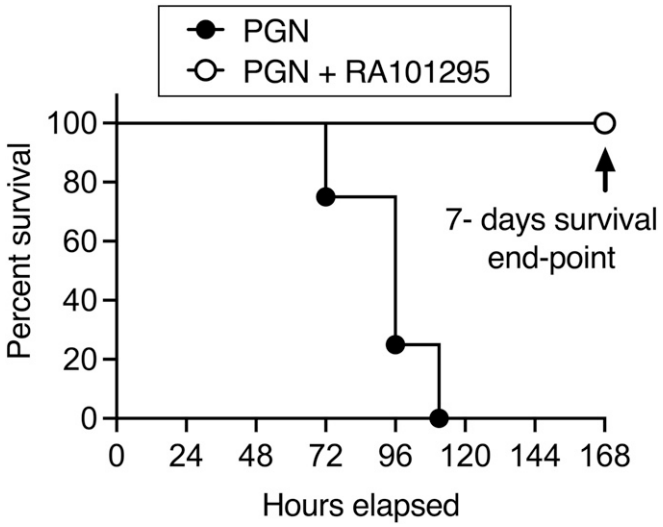

Fig. 7. Effect of RA101295 on PGN-induced mortality. Survival plot of animals challenged with PGN and treated with (n = 3) or without (n = 4) RA101295. Animals were monitored during the course of study and humanely euthanized when conditions deteriorated or reached at primary endpoint of 7 d (168 h, survivor). Survival distribution of the two groups was determined using a Log-rank (Mantel–Cox) test; the result is significant at P = 0.0169.

tests. Nevertheless, multiple anthrax strains, including atoxigenic and nonencapsulated isolates, show hemolytic activity against erythrocytes sensitized by mild reducing conditions (58) or phospholipase transfer (57), indicative of complement dysregulation. Our results demonstrate that anthrax hemolytic potential is driven by the cell wall PGN, which induces erythrolysis through direct and excessive activation of complement in the absence of any other bacterial PAMPs. The resulting anemia in anthrax patients could be further exacerbated through inhibition of erythropoiesis by lethal toxin (59). Since PGN is highly abundant in gram-positive pathogens, the mechanism depicted here could drive HUS in other bacterial infections and may explain the successful treatment of *Streptococcus pneumoniae* HUS using eculizumab (60), a C5-neutralizing antibody.

While optimal complement is beneficial in clearing infections, excessive complement activation amplifies sepsis pathology and contributes to cell death, immune paralysis, cardiopulmonary impairment, and multiple organ failure (61). We show here that anthrax PGN is a potent activator of all three complement cascades in baboons, leading to near-complete consumption of common pathway components as early as 1 h after PGN infusion. Although reported in vitro with a diverse array of bacterial cell walls and PGNs (62), the complementopathic potential of anthrax PGN in vivo has not been documented until now. During the course of *B. anthracis* infection, anthrax PGN can be released from bacteria during bacterial multiplication (25). Moreover, neutrophil-mediated extracellular killing of vegetative bacteria in the bacteremic stage (63, 64) could further amplify cell wall fragmentation and systemic release of PGN. Persistent PGN in circulation in turn may drive excessive complement activation, as we show here, and contribute to late-stage anthrax pathology including HUS. Similarly, PGN has been shown to persist long after Lyme infection and support post-infection inflammatory pathology (65).

Dysregulated activation of complement by PGN on RBC surfaces can be initiated by all three complement pathways (56, 66) and results in a rapid loss of hemoglobin and RBC fragmentation. Independent of MAC deposition (67), C3 opsonization of RBCs also enhances the erythro-phagocytic clearance at extravascular sites (68) and alters RBC membrane stiffness and deformability (69). Trafficking through partially thrombosed microvessels can promote schistiocytosis of stiff RBCs, which usually associates with DIC (46). By inhibiting C5 proteolysis without affecting upstream complement activation of C3, RA101295 discriminates between MAC- and C3-dependent hemolytic processes. In our current study, we observed early deposition of MAC on erythrocytes after PGN infusion. Hemolytic anemia started by 24 h, progressed throughout the course of the study in three of the four PGN-challenged baboons, and presented as intravascular hemolysis with schistocytosis and RBC fragmentation. C5b-9 deposition on RBCs drives PGN-induced hemolysis since RA101295 treatment normalized the hematocrit to 80% of baseline and reduced schistocytosis. C3 activation together with the progressive coagulopathy was largely unaffected by RA101295 but may still contribute to PGN-induced hemolysis to a lower extent. Indeed, RA101295-treated animals displayed mild anemia, and correspondingly mild kidney dysfunction, that resolved within a couple of days post challenge. RA101295-mediated protection of RBCs also resulted in lower clearance at extravascular sites, such as perifollicular regions in the spleen, despite higher C3b levels observed in these animals.

Sustained intravascular hemolysis leads to acute elevation of hemoglobin and/or heme in circulation, which exacerbates organ dysfunction in sepsis models (40) and associates with poor prognosis in patients (70). Heme accumulation propagates oxidative stress, induces inflammatory signaling through TLR4 and the NLRP3 inflammasome, induces neutrophil NETosis, and promotes macrophage necroptosis (reviewed in ref. 55). Extravascular heme accumulation is cytotoxic and sensitizes parenchymal cells to receptor-initiated necroptosis in the presence of inflammatory signals such as TNF (71) or exacerbates oxidative stress, primarily lipid peroxidation, and promotes ferroptosis (37). In vivo heme cytotoxicity predominantly associates with acute kidney injury (38) characterized by necrosis of renal epithelia in proximal tubules (39). Accordingly, PGN infusion in baboons induced tubular necrosis and preferential accumulation of iron in uriniferous tubules, indicative of heme-mediated damage. Renal injury here was amplified by a secondary deposition of C5b-9 complexes on uriniferous tubules. RA101295 treatment reduced hemolysis, renal cytotoxicity, and necrosis, eliminated iron deposition in proximal tubules, and protected against renal dysfunction. RA101295-treated animals showed little to no renal buildup of upstream complement initiators, immunoglobulins and/or MBL, suggesting that PGN-induced renal complement deposition occurs secondary to heme-mediated damage in this model.

Circulating innate immune cells recognize opsonized PGN through surface immune receptors like immunoglobulin and complement C3 receptors (22–26, 28). C3b opsonization contributes to phagocytosis of both live *B. anthracis* and PGN by neutrophils (24) and of *B. anthracis* spores by macrophages (34). Conversely, C5 inhibition did not impair C3b-mediated phagocytosis in our *E. coli* model (30); therefore, C5 inhibition was not expected to impede PGN recognition and initial activation of cellular innate responses by this PAMP. Accordingly, leukocyte and platelet dynamics, neutrophil degranulation and NETosis, induction of monocyte and lymphocyte mediators, including cytotoxic granzyme B produced by cytotoxic lymphocytes and NK cells (72), and early proinflammatory mediators were similar between RA101295-treated and nontreated animals.

The marked increase in neopterin produced by activated monocyte/macrophages under proinflammatory stimuli (73) observed in untreated, PGN-challenged animals reflects both sustained macrophage activation and impaired renal excretion, knowing that glomerular filtration is the main mechanism for neopterin clearance (41). This is in stark contrast with C5 inhibition during lethal *E. coli* challenge (30), in which all early proinflammatory molecules were reduced by RA101295. Whereas bacteriolytic MAC activity, sensitive to RA101295, led to LPS release from *E. coli* and subsequent LPS-driven inflammation in the gram-negative model, MAC activity

has no bearing on gram-positive PGN recognition by immune cells in the current study. Nevertheless, C5 inhibition significantly increased the early production of IFN-γ and reduced inflammatory mediators at later stages, such as IL-6, IL-10, and IL-1RA. These differences could reflect signaling contributions from the terminal complement mediators C5a and sC5b-9 (42, 43). C5a can induce IL-6 production (74, 75) through C5a-C5aR1 signaling (76) via ERK1/2 and p38 MAPK (77). Decreased signaling via C5a-C5aR1 in RA101295-treated baboons could be also responsible for IFN-γ induction and IL-10 decrease, as similar cytokine changes were found in C5aR1 knockout mice with polybacterial peritonitis (78). The diminished immune response could be also explained by the decrease in PGLYRP1 seen in RA101295-treated baboons, as this is a ligand of TREM1, and signaling through this receptor is known to promote the production of proinflammatory cytokines (79). We conclude that RA101295 does not interfere with immune recognition of PGN and supports a beneficial shift in systemic inflammation consistent with improved survival.

Concurrent activation of complement and blood coagulation occurs in many sepsis models, and the extensive crosstalk between them may contribute to hemostatic dysregulation, multiple organ failure, and mortality in sepsis (80). As reported (15), PGN activated both clotting cascades in baboons and induced a progressive consumptive coagulopathy leading to DIC. In contrast to C5 inhibition in gram-negative sepsis (30), RA101295 did not significantly alter the hemostatic dysregulation in PGN-challenged baboons, although a temporal delay in peak generation of protease–serpin complexes was observed in the treated group. We interpret these results as diminished amplification events in the presence of RA101295 due to inhibition of MAC activity on intravascular surfaces. Consequently, similar thrombin generation and fibrin formation were observed in PGN-challenged animals regardless of the presence of the C5 inhibitor. Although plasmin activation was similar between the two groups, fibrinolysis was enhanced in RA101295-treated animals at later time points, as shown by plasma D-dimers. While this finding is puzzling, the net fibrinolytic effect likely minimizes deposition of fibrin in the microvasculature with beneficial effects for thrombo-ischemic resolution and DIC-augmented hemolysis. In addition, RA101295 protected vascular endothelium from the excessive complement activation, as revealed by sTM levels. Lower endothelial activation slows clotting reactions and may decrease the thrombotic microangiopathy in this model.

Overall, we show that anthrax PGN induces a progressive HUS-like pathology similar to bacteremic human patients. Etiologically, direct excessive activation of complement, MAC-mediated hemolysis, heme imbalance, and associated renal injury promote acute kidney failure and death in anthrax PGN-challenged animals. Inhibition of C5 proteolysis prevents HUS pathology with no adverse effects on immune responses. Whereas the study provides proof-of-concept that dissociation of opsonophagocytic and cytolytic complement functions is beneficial for late-stage anthrax pathology, further work is needed to define the post-infection therapeutic windows in preclinical models.

Materials and Methods

NHP Model of Anthrax PGN Challenge. Animal study protocols were approved by the Institutional Animal Care and Use Committees of the Oklahoma Medical Research Foundation, the University of Oklahoma Health Sciences Center, and the University of Texas MD Anderson Cancer Center. All animal experiments were performed in compliance with the Animal Welfare Act, the Guide for the Care and Use of Laboratory Animals (81), and the NIH Office of Laboratory Animal Welfare. Healthy, male and female, 3- to 4-y-old *Papio anubis* baboons with hemoglobin greater than 10 g/dL and WBC counts less than 12×10^9/L were randomly distributed between two study groups. All animals had free access to water and primate diet. Animals were sedated with intramuscular (IM) ketamine (14-20 mg/kg), after which intravenous (IV) pentobarbital (2 mg/kg) was used to maintain a light level of anesthesia during the first 8 h after the PGN challenge. The animals were returned to cage for recovery afterward. Buprenorphine (0.02 mg/kg, IM) was administered after 6 h of PGN challenge. Two experimental groups were studied: 1) PGN challenge only (n = 4) and 2) PGN plus RA101295 treatment (n = 3). Anthrax PGN was prepared and characterized as described elsewhere (15, 21) and was infused IV over 15 min (37.5 mg/kg). Four doses of RA101295 (10 mg/kg) were administered subcutaneously in order to ensure inhibition of C5 proteolysis throughout the first 2 d after the challenge, as described elsewhere (30). Blood and physiological parameters were collected during the course of study. Mean systemic arterial pressure, heart rate, respiratory rate, core body temperature, and oxygen saturation were monitored with a Cardell Max12 HD Duo monitor (Midmark, Versailles, OH). Supplemental oxygen was given when oxygen saturation dropped below 85%. Animals were monitored during the course of study and humanely euthanized when conditions deteriorated or reached the primary endpoint of 7 d survival (14, 82). Tissue samples were fixed in 4% paraformaldehyde for microscopy or snap frozen in liquid nitrogen and stored at −80 °C.

Biochemical Tests. Blood lactate was measured using lactate Scout (EKF Diagnostics GmbH, Barleben, Germany). Blood glucose was measured using a Contour Next blood glucose meter (Bayer HealthCare LLC, Mishawaka, IN). Serum metabolites such as BUN, creatinine, alanine aminotransferase, total protein, and albumin were measured using a comprehensive diagnostic profile rotor on a VetScan VS2 (Abaxis Veterinary Diagnostics, Union City, CA) chemistry analyzer. Plasma MPO activity was quantified using the FluoroMPO MPO detection kit (Cell Technology, Fremont, CA) according to manufacturer's protocol.

Coagulation Tests. aPTT, PT, and functional fibrinogen was determined using clotting based assays (83).

Enzyme-Linked Immunoassays. Plasma cytokines were quantified using a customized MILLIPLEX MAP Non-Human Primate Cytokine Magnetic Bead Panel (EMD Millipore, Billerica, MA) as per manufacturer's instruction. C3b, C5a, and C5b-9 were quantified as described (30, 84). Wieslab total complement screening kit (Euro Diagnostica, Malmö, Sweden) was used to assess pathways specific complement activities (85), according to manufacturer's instructions. This kit detects the residual complement components that support complement activation through the three activation pathways. Serum is incubated in wells coated with specific activators of the three pathways: human IgM for CP, LPS for AP, and mannan for LP. Complement activation readout is C5b-9 terminal complex formation measured with a specific, neo-epitope–based, enzyme-linked immunosorbent assay (ELISA). The amount of neoantigen generated is proportional to the residual functional activity of each specific complement pathway. Antithrombin complexes with FXIIa, kallikrein (Kal), and FVIIa were quantified as described (86), and values were interpolated from standards prepared by incubating lepirudin-anticoagulated baboon plasma with either 0.1 mg/mL dextran sulfate (for FXIIa-AT and Kal-AT) or PT reagent (for FVIIa-AT) for 60 min at 37 °C. Plasma intact kininogen levels were measured by ELISA using a kininogen capture antibody (clone 3E8) and biotinylated kininogen detection antibody (clone 2B7) as described elsewhere (87) and interpolated from a standard curve generated using single-chain, high–molecular weight kininogen (Molecular Innovations, Novi, MI). PAP complexes and D-dimers were quantified as described earlier (86). tPA, PAI-1, and granzyme B were quantified using commercial ELISA kits (R&D System, Minneapolis, MN). Neopterin ELISA kit was from IBL International GmbH (Hamburg, Germany). Plasma nucleosomes were quantified using a Cell Death Detection ELISA PLUS kit (Roche Diagnostics GmbH, Mannheim, Germany) with nucleohistones (Worthington Biochemical Corporation, Lakewood, NJ) as standard.

Western Blotting. Plasma samples were mixed with NuPAGE lithium dodecylsulfate (LDS) sample buffer (Invitrogen, Carlsbad, CA) and heated at 70 °C for 10 min. Samples were applied to NuPAGE 4 to 12% Bis-Tris gels (Invitrogen) and electrophoresed at constant 200V for 45 min using NuPAGE MES-SDS (2-(N-morpholino)-ethanesulfonic acid - sodium dodecylsulfate) running buffer under nonreducing condition. Proteins were transferred to polyvinylidene difluoride (PVDF) membranes at constant 30V for 75 min using NuPAGE transfer buffer (Invitrogen) with 20% methanol. Membranes were blocked with 3% bovine serum albumin (BSA) in saline phosphate buffer (PBS) containing 0.1% Tween-20 for 2 h and then incubated with either goat anti-human PGLYRP1 (0.4 μg/mL, R&D systems) or rabbit anti-human PGLYRP2 (0.4 μg/mL, Novus Biologicals, Littleton, CO) at 4 °C overnight. After 1-h incubation with respective secondary antibody Alexa Fluor 680 conjugated donkey anti-goat IgG (200 ng/mL, Molecular Probes, Eugene, OR) or IRDye 680RD conjugated donkey anti-rabbit IgG (66 ng/mL, Li-Cor

Biosciences, Lincoln, NE), membranes were scanned using the Odyssey infrared imaging system (Li-Cor Biosciences) in a 700-nm channel.

Microscopy Analysis. Formalin-fixed, paraffin-embedded sections were stained with hematoxylin and eosin or phosphotungstic acid–hematoxylin and were examined and scored by a veterinary pathologist blinded to the experimental condition. Prussian blue staining of hemosiderin deposits (ferric iron) was performed as described (14, 30, 83).

Immunofluorescent staining was performed on methanol-fixed blood smears or paraformaldehyde-fixed tissues embedded in Tissue-Tek OCT compound (Sakura Finetek, Torrance, CA). Samples were incubated overnight at 4 °C with neoepitope-specific mouse anti-human C5b-9 (clone aE11; Enzo Life Sciences, Farmingdale, NY), rabbit anti- human mannose MBL (clone EPSISR5; Epitomics, Burlingame, CA), rabbit anti-human complement factor B (Novus Biologicals), or rabbit anti- human IgA/IgG/IgM polyclonal antibody (Dako, Santa Clara, CA). Sections were subsequently washed and incubated for 1 h with fluorescein isothiocyanate- and/or Cy3-conjugated detection antibodies (Jackson ImmunoResearch Laboratories, West Grove, PA) and mounted with Vectashield hardset (Vector Laboratories, Burlingame, CA) containing TO-PRO-3 iodine (Molecular Probes, Eugene, OR) nuclear counterstain. Confocal images were captured on a Nikon Eclipse TE2000-U inverted microscope (Nikon Instruments Inc., Melville, NY), equipped with a Nikon C1 scanning head, and processed using EZ-C1 software (version 3.80; Nikon, Melville NY) (30, 83).

Statistical Analysis. Data are represented as mean ± SEM). Statistical analysis was performed using GraphPad Prism version 8.4.3 (GraphPad Software, San Diego). Significant deviations from baseline (T0) were assessed by repeated-measures one-way ANOVA with Tukey's correction for multiple comparisons. Differences between the two experimental groups were assessed by multiple *t* tests. Results were considered significant at $P < 0.05$ ($^{*}P < 0.05$, $^{**}P < 0.01$, and $^{***}P < 0.001$). Comparison of survival data were done using the log-rank (Mantel–Cox) test.

Data Availability. All study data are included in the article and/or *SI Appendix*.

ACKNOWLEDGMENTS. This research was funded by the National Institute for General Medical Sciences grants GM121601 (F.L.) and GM122775 (F.L.) and the National Institute of Allergy and Infectious Diseases grants U19AI062629 (K.M.C.) and AI157037 (F.L.). The Baboon Research Resource is supported by NIH award P40OD024628 (J.H.S). RA101295 compound was provided by Ra Pharmaceuticals. Antibodies against intact and cleaved kininogen were provided by Dr. Sidney Strickland (Rockefeller University). The content is solely the responsibility of the authors and does not necessarily represent the official views of the NIH or Ra Pharmaceuticals.

1. D. A. Sweeney, C. W. Hicks, X. Cui, Y. Li, P. Q. Eichacker, Anthrax infection. *Am. J. Respir. Crit. Care Med.* **184**, 1333–1341 (2011).
2. C. J. Carlson *et al*., The global distribution of Bacillus anthracis and associated anthrax risk to humans, livestock and wildlife. *Nat. Microbiol.* **4**, 1337–1343 (2019).
3. M. G. Walsh, A. W. de Smalen, S. M. Mor, Climatic influence on anthrax suitability in warming northern latitudes. *Sci. Rep.* **8**, 9269 (2018).
4. T. V. Inglesby *et al*.; Working Group on Civilian Biodefense, Anthrax as a biological weapon, 2002: Updated recommendations for management. *JAMA* **287**, 2236–2252 (2002).
5. A. R. Hoffmaster *et al*., Identification of anthrax toxin genes in a Bacillus cereus associated with an illness resembling inhalation anthrax. *Proc. Natl. Acad. Sci. U.S.A.* **101**, 8449–8454 (2004).
6. S. Dupke *et al*., Serological evidence for human exposure to Bacillus cereus biovar anthracis in the villages around Taï National Park, Côte d'Ivoire. *PLoS Negl. Trop. Dis.* **14**, e0008292 (2020).
7. S. R. Klee *et al*., Characterization of Bacillus anthracis-like bacteria isolated from wild great apes from Cote d'Ivoire and Cameroon. *J. Bacteriol.* **188**, 5333–5344 (2006).
8. A. M. Wright *et al*., Rapidly progressive, fatal, inhalation anthrax-like infection in a human: Case report, pathogen genome sequencing, pathology, and coordinated response. *Arch. Pathol. Lab. Med.* **135**, 1447–1459 (2011).
9. T. Candela, A. Fouet, Poly-gamma-glutamate in bacteria. *Mol. Microbiol.* **60**, 1091–1098 (2006).
10. M. Moayeri, S. H. Leppla, Cellular and systemic effects of anthrax lethal toxin and edema toxin. *Mol. Aspects Med.* **30**, 439–455 (2009).
11. L. M. Grinberg, F. A. Abramova, O. V. Yampolskaya, D. H. Walker, J. H. Smith, Quantitative pathology of inhalational anthrax I: Quantitative microscopic findings. *Mod. Pathol.* **14**, 482–495 (2001).
12. J. Guarner *et al*.; Inhalational Anthrax Pathology Working Group, Pathology and pathogenesis of bioterrorism-related inhalational anthrax. *Am. J. Pathol.* **163**, 701–709 (2003).
13. J. A. Jernigan *et al*.; Anthrax Bioterrorism Investigation Team, Bioterrorism-related inhalational anthrax: The first 10 cases reported in the United States. *Emerg. Infect. Dis.* **7**, 933–944 (2001).
14. D. J. Stearns-Kurosawa, F. Lupu, F. B. Taylor Jr, G. Kinasewitz, S. Kurosawa, Sepsis and pathophysiology of anthrax in a nonhuman primate model. *Am. J. Pathol.* **169**, 433–444 (2006).
15. N. I. Popescu *et al*., Peptidoglycan induces disseminated intravascular coagulation in baboons through activation of both coagulation pathways. *Blood* **132**, 849–860 (2018).
16. P. Qiu *et al*., Bacillus anthracis cell wall peptidoglycan but not lethal or edema toxins produces changes consistent with disseminated intravascular coagulation in a rat model. *J. Infect. Dis.* **208**, 978–989 (2013).
17. K. H. Schleifer, O. Kandler, Peptidoglycan types of bacterial cell walls and their taxonomic implications. *Bacteriol. Rev.* **36**, 407–477 (1972).
18. M. Chamaillard *et al*., An essential role for NOD1 in host recognition of bacterial peptidoglycan containing diaminopimelic acid. *Nat. Immunol.* **4**, 702–707 (2003).
19. S. E. Girardin *et al*., Nod2 is a general sensor of peptidoglycan through muramyl dipeptide (MDP) detection. *J. Biol. Chem.* **278**, 8869–8872 (2003).
20. A. J. Wolf *et al*., Hexokinase Is an Innate Immune Receptor for the Detection of Bacterial Peptidoglycan. *Cell* **166**, 624–636 (2016).
21. M. Langer *et al*., Neither Lys- and DAP-type peptidoglycans stimulate mouse or human innate immune cells via Toll-like receptor 2. *PLoS One* **13**, e0193207 (2018).
22. D. Sun *et al*., Anti-peptidoglycan antibodies and Fcγ receptors are the key mediators of inflammation in Gram-positive sepsis. *J. Immunol.* **189**, 2423–2431 (2012).
23. D. Sun *et al*., Bacillus anthracis peptidoglycan activates human platelets through FcγRII and complement. *Blood* **122**, 571–579 (2013).
24. N. I. Popescu, R. S. Keshari, J. Cochran, K. M. Coggeshall, F. Lupu, C3 opsonization of anthrax bacterium and peptidoglycan supports recognition and activation of neutrophils. *Microorganisms* **8**, 1039 (2020).
25. J. K. Iyer *et al*., Inflammatory cytokine response to Bacillus anthracis peptidoglycan requires phagocytosis and lysosomal trafficking. *Infect. Immun.* **78**, 2418–2428 (2010).
26. A. W. Girton *et al*., Serum amyloid P and IgG exhibit differential capabilities in the activation of the innate immune system in response to Bacillus anthracis peptidoglycan. *Infect. Immun.* **86**, e00076-18 (2018).
27. M. Langer *et al*., Bacillus anthracis peptidoglycan stimulates an inflammatory response in monocytes through the p38 mitogen-activated protein kinase pathway. *PLoS One* **3**, e3706 (2008).
28. N. I. Popescu, A. Girton, T. Burgett, K. Lovelady, K. M. Coggeshall, Monocyte procoagulant responses to anthrax peptidoglycan are reinforced by proinflammatory cytokine signaling. *Blood Adv.* **3**, 2436–2447 (2019).
29. J. K. Iyer, K. M. Coggeshall, Cutting edge: Primary innate immune cells respond efficiently to polymeric peptidoglycan, but not to peptidoglycan monomers. *J. Immunol.* **186**, 3841–3845 (2011).
30. R. S. Keshari *et al*., Inhibition of complement C5 protects against organ failure and reduces mortality in a baboon model of *Escherichia coli* sepsis. *Proc. Natl. Acad. Sci. U.S.A.* **114**, E6390–E6399 (2017).
31. A. Freedman *et al*., Cutaneous anthrax associated with microangiopathic hemolytic anemia and coagulopathy in a 7-month-old infant. *JAMA* **287**, 869–874 (2002).
32. A. G. Wu *et al*., Anthrax toxin induces hemolysis: An indirect effect through polymorphonuclear cells. *J. Infect. Dis.* **188**, 1138–1141 (2003).
33. M. Gallegos-Candela *et al*., Validated MALDI-TOF-MS method for anthrax lethal factor provides early diagnosis and evaluation of therapeutics. *Anal. Biochem.* **543**, 97–107 (2018).
34. C. Premanandan *et al*., Complement protein C3 binding to Bacillus anthracis spores enhances phagocytosis by human macrophages. *Microb. Pathog.* **46**, 306–314 (2009).
35. D. N. Kyriacou *et al*., Clinical predictors of bioterrorism-related inhalational anthrax. *Lancet* **364**, 449–452 (2004).
36. R. Larsen, Z. Gouveia, M. P. Soares, R. Gozzelino, Heme cytotoxicity and the pathogenesis of immune-mediated inflammatory diseases. *Front. Pharmacol.* **3**, 77 (2012).
37. S. J. Dixon, B. R. Stockwell, The role of iron and reactive oxygen species in cell death. *Nat. Chem. Biol.* **10**, 9–17 (2014).
38. E. Tolosano *et al*., Defective recovery and severe renal damage after acute hemolysis in hemopexin-deficient mice. *Blood* **94**, 3906–3914 (1999).
39. A. Zarjou *et al*., Proximal tubule H-ferritin mediates iron trafficking in acute kidney injury. *J. Clin. Invest.* **123**, 4423–4434 (2013).
40. R. Larsen *et al*., A central role for free heme in the pathogenesis of severe sepsis. *Sci. Transl. Med.* **2**, 51ra71 (2010).
41. H. Y. Lhee, H. Kim, K. J. Joo, S. S. Jung, K. B. Lee, The clinical significance of serum and urinary neopterin levels in several renal diseases. *J. Korean Med. Sci.* **21**, 678–682 (2006).
42. H. Montz, K. C. Koch, R. Zierz, O. Götze, The role of C5a in interleukin-6 production induced by lipopolysaccharide or interleukin-1. *Immunology* **74**, 373–379 (1991).
43. C. Viedt, G. M. Hänsch, R. P. Brandes, W. Kübler, J. Kreuzer, The terminal complement complex C5b-9 stimulates interleukin-6 production in human smooth muscle cells through activation of transcription factors NF-kappa B and AP-1. *FASEB J.* **14**, 2370–2372 (2000).
44. A. J. Wolf, D. M. Underhill, Peptidoglycan recognition by the innate immune system. *Nat. Rev. Immunol.* **18**, 243–254 (2018).
45. P. Sharma *et al*., Crystal structure of the peptidoglycan recognition protein at 1.8 A resolution reveals dual strategy to combat infection through two independent functional homodimers. *J. Mol. Biol.* **378**, 923–932 (2008).
46. J. F. Lesesve *et al*., Schistocytes in disseminated intravascular coagulation. *Int. J. Lab. Hematol.* **36**, 439–443 (2014).

47. J. Reith, C. Mayer, Peptidoglycan turnover and recycling in Gram-positive bacteria. *Appl. Microbiol. Biotechnol.* **92**, 1–11 (2011).
48. P. van Langevelde *et al*., Antibiotic-induced release of lipoteichoic acid and peptidoglycan from Staphylococcus aureus: Quantitative measurements and biological reactivities. *Antimicrob. Agents Chemother.* **42**, 3073–3078 (1998).
49. S. A. Ragland, A. K. Criss, From bacterial killing to immune modulation: Recent insights into the functions of lysozyme. *PLoS Pathog.* **13**, e1006512 (2017).
50. S. J. Hayden, T. J. Albert, T. R. Watkins, E. R. Swenson, Anemia in critical illness: Insights into etiology, consequences, and management. *Am. J. Respir. Crit. Care Med.* **185**, 1049–1057 (2012).
51. G. F. Muady *et al*., Hemoglobin levels and blood transfusion in patients with sepsis in internal medicine departments. *BMC Infect. Dis.* **16**, 569 (2016).
52. A. Joseph, A. Cointe, P. Mariani Kurkdjian, C. Rafat, A. Hertig, Shiga toxin-associated hemolytic uremic syndrome: A narrative review. *Toxins* **12**, 67 (2020).
53. J. M. Spinale, R. L. Ruebner, B. S. Kaplan, L. Copelovitch, Update on Streptococcus pneumoniae associated hemolytic uremic syndrome. *Curr. Opin. Pediatr.* **25**, 203–208 (2013).
54. B. Mina *et al*., Fatal inhalational anthrax with unknown source of exposure in a 61-year-old woman in New York City. *JAMA* **287**, 858–862 (2002).
55. K. Van Avondt, E. Nur, S. Zeerleder, Mechanisms of haemolysis-induced kidney injury. *Nat. Rev. Nephrol.* **15**, 671–692 (2019).
56. K. Effenberger-Neidnicht, M. Hartmann, Mechanisms of hemolysis during sepsis. *Inflammation* **41**, 1569–1581 (2018).
57. A. P. Pomerantsev, N. A. Staritsin, Mockov YuV, L. I. Marinin, , Expression of cereolysine AB genes in Bacillus anthracis vaccine strain ensures protection against experimental hemolytic anthrax infection. *Vaccine* **15**, 1846–1850 (1997).
58. P. F. Fellows, A survey of worldwide strains of Bacillus anthracis. *Salisbury Med. Bull.* **87S**, 31–33 (1996).
59. H. H. Chang *et al*., Erythropoiesis suppression is associated with anthrax lethal toxin-mediated pathogenic progression. *PLoS One* **8**, e71718 (2013).
60. G. Jeantet *et al*., Successful treatment of a *Streptococcus pneumoniae*-associated haemolytic uraemic syndrome by eculizumab. *Clin. Kidney J.* **12**, 106–109 (2019).
61. D. Rittirsch, M. A. Flierl, P. A. Ward, Harmful molecular mechanisms in sepsis. *Nat. Rev. Immunol.* **8**, 776–787 (2008).
62. A. Kawasaki *et al*., Activation of the human complement cascade by bacterial cell walls, peptidoglycans, water-soluble peptidoglycan components, and synthetic muramylpeptides–studies on active components and structural requirements. *Microbiol. Immunol.* **31**, 551–569 (1987).
63. A. Mayer-Scholl *et al*., Human neutrophils kill Bacillus anthracis. *PLoS Pathog.* **1**, e23 (2005).
64. J. Z. Liu, S. R. Ali, E. Bier, V. Nizet, Innate immune interactions between *Bacillus anthracis* and host neutrophils. *Front. Cell. Infect. Microbiol.* **8**, 2 (2018).
65. B. L. Jutras *et al*., *Borrelia burgdorferi* peptidoglycan is a persistent antigen in patients with Lyme arthritis. *Proc. Natl. Acad. Sci. U.S.A.* **116**, 13498–13507 (2019).
66. R. A. Brodsky, Complement in hemolytic anemia. *Blood* **126**, 2459–2465 (2015).
67. R. Notaro, M. Sica, C3-mediated extravascular hemolysis in PNH on eculizumab: Mechanism and clinical implications. *Semin. Hematol.* **55**, 130–135 (2018).
68. Z. Lin *et al*., Complement C3dg-mediated erythrophagocytosis: Implications for paroxysmal nocturnal hemoglobinuria. *Blood* **126**, 891–894 (2015).
69. K. L. Sung, J. Freedman, A. Chabanel, S. Chien, Effect of complement on the viscoelastic properties of human erythrocyte membrane. *Br. J. Haematol.* **61**, 455–466 (1985).
70. D. R. Janz *et al*., Association between cell-free hemoglobin, acetaminophen, and mortality in patients with sepsis: An observational study. *Crit. Care Med.* **41**, 784–790 (2013).
71. E. Seixas *et al*., Heme oxygenase-1 affords protection against noncerebral forms of severe malaria. *Proc. Natl. Acad. Sci. U.S.A.* **106**, 15837–15842 (2009).
72. S. Zeerleder *et al*., Activated cytotoxic T cells and NK cells in severe sepsis and septic shock and their role in multiple organ dysfunction. *Clin. Immunol.* **116**, 158–165 (2005).
73. J. Gómez-Jiménez *et al*., Interleukin-10 and the monocyte/macrophage-induced inflammatory response in septic shock. *J. Infect. Dis.* **171**, 472–475 (1995).
74. M. Ji *et al*., C5a induces the synthesis of IL-6 and TNF-α in rat glomerular mesangial cells through MAPK signaling pathways. *PLoS One* **11**, e0161867 (2016).
75. J. M. Pobanz, R. A. Reinhardt, S. Koka, S. D. Sanderson, C5a modulation of interleukin-1 beta-induced interleukin-6 production by human osteoblast-like cells. *J. Periodontal Res.* **35**, 137–145 (2000).
76. Y. Liu, S. Q. Xu, W. J. Long, X. Y. Zhang, H. L. Lu, C5aR antagonist inhibits occurrence and progression of complement C5a induced inflammatory response of microglial cells through activating p38MAPK and ERK1/2 signaling pathway. *Eur. Rev. Med. Pharmacol. Sci.* **22**, 7994–8003 (2018).
77. N. C. Riedemann *et al*., Regulatory role of C5a in LPS-induced IL-6 production by neutrophils during sepsis. *FASEB J.* **18**, 370–372 (2004).
78. O. Sommerfeld *et al*., Targeting complement C5a receptor 1 for the treatment of immunosuppression in sepsis. *Mol. Ther.* **29**, 338–346 (2021).
79. C. B. Read *et al*., Cutting edge: Identification of neutrophil PGLYRP1 as a ligand for TREM-1. *J. Immunol.* **194**, 1417–1421 (2015).
80. F. Lupu, R. S. Keshari, J. D. Lambris, K. M. Coggeshall, Crosstalk between the coagulation and complement systems in sepsis. *Thromb. Res.* **133**, S28–S31 (2014).
81. N. R. Council, *Guide for the Care and Use of Laboratory Animals* (The National Academies Press, Washington, DC, ed. 8, 2011), pp. 246, 10.17226/12910.
82. F. B. Taylor Jr, G. T. Kinasewitz, F. Lupu, Pathophysiology, staging and therapy of severe sepsis in baboon models. *J. Cell. Mol. Med.* **16**, 672–682 (2012).
83. R. Silasi-Mansat *et al*., Complement inhibition decreases the procoagulant response and confers organ protection in a baboon model of Escherichia coli sepsis. *Blood* **116**, 1002–1010 (2010).
84. G. Bergseth *et al*., An international serum standard for application in assays to detect human complement activation products. *Mol. Immunol.* **56**, 232–239 (2013).
85. E. B. Volokhina *et al*., Sensitive, reliable and easy-performed laboratory monitoring of eculizumab therapy in atypical hemolytic uremic syndrome. *Clin. Immunol.* **160**, 237–243 (2015).
86. R. Silasi *et al*., Inhibition of contact-mediated activation of factor XI protects baboons against *S aureus*-induced organ damage and death. *Blood Adv.* **3**, 658–669 (2019).
87. H. Yamamoto-Imoto *et al*., A novel detection method of cleaved plasma high-molecular-weight kininogen reveals its correlation with Alzheimer's pathology and cognitive impairment. *Alzheimers Dement. (Amst.)* **10**, 480–489 (2018).